

Benzoquinolateplatinum(II) complexes as building blocks in the synthesis of Pt–Ag extended structures†

Juan Forniés,^a Susana Ibáñez,^a Elena Lalinde,^{*b} Antonio Martín,^{*a} M. Teresa Moreno^b and Athanassios C. Tsipis^{*c}

Received 6th October 2011, Accepted 23rd December 2011

DOI: 10.1039/c2dt11885h

The reaction between (NBu₄)[Pt(bzq)(C₆F₅)₂] (**1**, bzq = 7,8-benzoquinolate) and AgClO₄ in a 1 : 1 molar ratio, in acetone, gives the polymer [Pt(bzq)(C₆F₅)₂Ag]_n (**2**). The reaction of **2** with equimolecular amounts of PPh₃ and SC₄H₈ (tht) produces the bimetallic complexes [Pt(bzq)(C₆F₅)₂AgL] (L = PPh₃ (**3**), tht (**4**)). For L = py, decomposition takes place and [Pt(bzq)(C₆F₅)py] (**5**) is obtained. All these complexes have been characterized by X-ray diffraction. The most interesting features of complexes **2–4** is the presence of Pt–Ag bonds, with Pt–Ag distances of *ca.* 2.75 Å. Besides, the silver centres establish short η¹ bonding interactions with the C_{ipso} of the bzq ligands, with distances Ag–C of *ca.* 2.45 Å. Complex **2** is a one-dimensional infinite chain in which the fragments “Pt(bzq)(C₆F₅)₂” and Ag⁺ alternate. On the other hand, complexes **1** and **3–5** show intermolecular pairing through π⋯π interactions between the aromatic rings of the bzq ligand, having interplanar separations of *ca.* 3.5 Å. Complex **2** dissolves in donor solvents (acetone, THF) as discrete bimetallic solvated fragments [Pt(bzq)(C₆F₅)₂AgS_n] (S = solvent), similar to complexes **3** and **4**. The persistence of the Pt–Ag bond in **2–4**, supported by multinuclear NMR spectroscopy, causes a significant blue-shift in the lowest-lying absorption in relation to **1**. This fact is attributed (TD-DFT) to a remarkable modification of the orbitals contributing to the HOMO, which changes the character of the transition from ¹LC/¹MLCT in **1** to admixture ¹L′LCT/¹MLCT in the bimetallic complexes. The low energy feature (490–530 nm) of **2** in solid state is attributed to CT from the Pt fragments to the Ag centers. Complexes **2–4** are only emissive in rigid media (solid and glasses). In the solid state, the metallic chain **2** exhibits a bright orange emission (560 nm, 298 K; 590 nm, 77 K), assigned to an excited state involving charge transfer from the platinum fragment with a remarkable contribution of C₆F₅ (Ar_F) rings to the Pt–Ag bond (³LMM′CT/³L′M′CT). However, **3** and **4** exhibit in solid state at 298 K a vibronic band, which is clearly resolved in two close non-equilibrated bands at 77 K in **3**, tentatively ascribed to a mixture of ³MLCT/³L′LCT transitions modified by the formation of the Pt–Ag bond. In glassy solution (77 K) **2–4** display a vibronic emission ascribed primarily to ³LC character.

Introduction

In the widely studied field of intermetallic bonds, metallophilic interactions between closed shell (d¹⁰, d⁸, d¹⁰s²) ions have attracted a considerable amount of attention.^{1–12} Among these types of interactions, the particular case of M(d⁸)→M′ dative bonds has been found in a rich variety of systems, mostly involving electron rich Pt(II) complexes as a framework donor involving the occupied d_{z²} orbital.^{5,13–31}

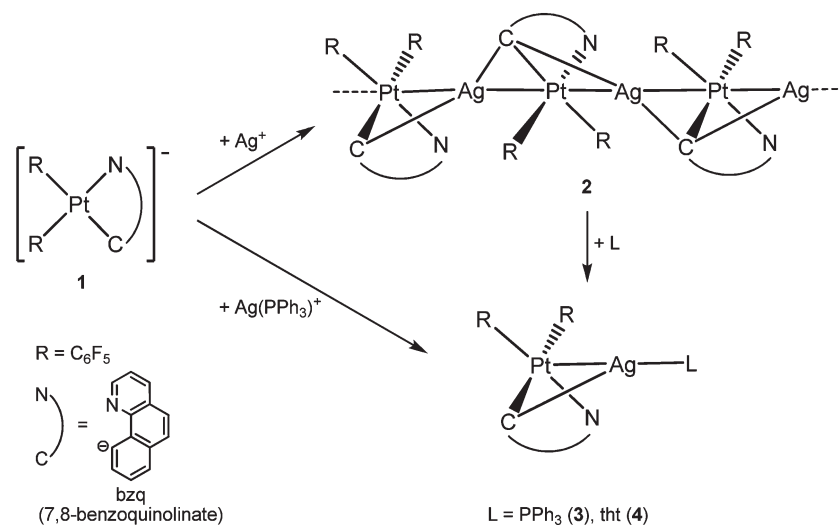
Heteropolymetallic complexes containing this kind of bond³² are interesting for several reasons. One is the utility of the metal–metal bond as a tool in molecular or crystal engineering. Thus, it is possible to find in the literature examples of a wide array of structure types in which the metal–metal bond links together the different subassemblies: linear bimetallic compounds,^{16,17,22,24} trimetallic “sandwiches”^{16–18,24,30} or triangles,^{33–35} tetrametallic “squares”^{15,19,24} or tetrahedrons,^{35–37} octanuclear stellate,³⁸

^aDepartamento de Química Inorgánica – Instituto de Síntesis Química y Catálisis Homógena. Universidad de Zaragoza – C.S.I.C., 50009 Zaragoza, Spain. E-mail: tello@unizar.es

^bDepartamento de Química – Grupo de Síntesis Química de La Rioja, UA–C.S.I.C. Universidad de La Rioja, 26006 Logroño, Spain

^cLaboratory of Inorganic and General Chemistry, Department of Chemistry, University of Ioannina, 451 10 Ioannina, Greece and Departamento de Química Inorgánica – Instituto de Ciencia de Materiales de Aragón. Universidad de Zaragoza – C.S.I.C., 50009 Zaragoza, Spain (on sabbatical leave)

† Electronic supplementary information (ESI) available: Complete authors list for ref. 94. X-ray structural drawings and data for complexes **3** and **5** (Fig. S1–S2 and Tables S1–S3). Normalized absorption spectra calculated from their reflectance diffuse spectra of **1**, **2** and **4** in solid state (Fig. S3). Details on the theoretical calculations carried out in **1–3** and **4** (Fig. S4–S9 and Tables S4–S11). CCDC reference numbers 847963–847967. For ESI and crystallographic data in CIF or other electronic format see DOI: 10.1039/c2dt11885h



Scheme 1

oligometallic “chains”,^{23,24} infinite one-dimensional chains³⁰ that sometimes arrange in helical motifs in the crystal structure,²³ *etc.* Besides, complexes containing Pt–Ag bonds have been shown to act as intermediates in halogen abstraction¹⁴ or Pt–C cleavage reactions.³⁹ Finally, some of these complexes exhibit interesting photophysical and photochemical properties,^{1–10,18,31,40–52} which in some cases have been exclusively attributed to the presence of metallophilic bonds. In other polymetallic systems based on potential emissive polydentate groups (alkynyl,^{53–56} thiolate,⁵⁴ pyrazolate^{57–59}...), the presence of metallophilic bonds also plays a crucial role in their final luminescent properties.

In the course of our current research, we have developed synthetic methods for the preparation of complexes containing Pt–M bonds, mainly based on the use of perhalophenyl platinate(II) complexes.^{13,16,17,34,37,38,60–63} Following our interest in this area, we are now interested in exploring the synthesis and properties of heteropolymetallic complexes based on anionic platinate building blocks containing typical strong ligand field cyclometalated C[^]N phosphors.^{5,15–18,64,65} Thus, we have shown that by using the properties of the basic platinum(II) centre as a Lewis base in the anionic complex (NBu₄)[Pt(bzq)(C₆X₅)₂] (X = F, 1; Cl; bzq = 7,8-benzoquinolate), several luminescent complexes stabilized by unsupported Pt–M (M = Cd, Ag) bonds can be easily generated.^{16,17} A few years ago we reported several bi- and trinuclear complexes containing Pt–Ag bonds¹⁷ and very unusual η^1 bonding interactions between the silver(I) centre and the C_{ipso} of the bzq ligand and additionally stabilized by short or long-range $\pi \cdots \pi$ stacking interactions between the aromatic rings of the bzq ligands. All these complexes exhibited interesting photoluminescent properties, including the occurrence of a luminescence polymorphism associated to the trinuclear “sandwich” complex (NBu₄)[{Pt(bzq)(C₆F₅)₂}₂Ag].

In this paper we expand our study on the ability of the synthon [Pt(bzq)(C₆F₅)₂][–] to form new complexes of diverse nuclearity containing Pt–Ag bonds. We have achieved the preparation of a one-dimensional polymer containing an infinite chain of formula [Pt(bzq)(C₆F₅)₂Ag]_n (**2**). The reactivity of **2** has been investigated and the cleavage of the chain with ligands

L has allowed the synthesis of complexes of stoichiometry [Pt(bzq)(C₆F₅)₂}AgL]. The reported complexes have been characterised and studied by X-ray crystallography and NMR spectroscopy. Finally, their optical properties have been investigated and time-dependent density functional theory (TD-DFT) calculations have been performed to shed light on the nature of the electronic transitions.

Results and discussion

Synthesis and characterization

As we have already mentioned, we reported that the reaction of (NBu₄)[Pt(bzq)(C₆F₅)₂] (**1**) with AgClO₄ in 2 : 1 (or even in 1 : 1) molar ratio in acetone results in the isolation of the trinuclear “sandwich” complex (NBu₄)[{Pt(bzq)(C₆F₅)₂}₂Ag].¹⁷ However, if this reaction is carried out in a 1 : 1 molar ratio in acetone and the solid resulting after evaporation to dryness is treated with CH₂Cl₂, a yellow solid of formula [Pt(bzq)(C₆F₅)₂}Ag] is obtained from the solution (see Experimental section). The X-ray crystal structure of this complex (see below) has revealed its polymeric nature [Pt(bzq)(C₆F₅)₂}Ag]_n (**2**) (see Scheme 1).

The molecular structures of **1** and **2** have been established by X-ray diffraction studies. Fig. 1 shows the complex anion of **1** and Table 1 lists its most relevant bond distances and angles. The most important feature found in the structure of **1** is the pairing of anions through $\pi \cdots \pi$ interactions of the bzq ligand. The two [Pt(bzq)(C₆F₅)₂][–] units stack their bzq planes (interplanar distance of *ca.* 3.6 Å) with the bulky C₆F₅ ligands oriented in the opposite direction in order to avoid steric hindrance. This $\pi \cdots \pi$ stacking has already been described in some neutral and cationic benzoquinolate platinum complexes,^{15–18,66–71} but is rather uncommon in anionic systems with bulky counter cations such as [NBu₄]⁺.

More interesting is the crystal structure of **2**, a view of which is presented in Fig. 2. Table 2 contains the most important bond lengths and angles. Complex **2** is a one-dimensional infinite chain in which the fragments “[Pt(bzq)(C₆F₅)₂][–]” and Ag⁺

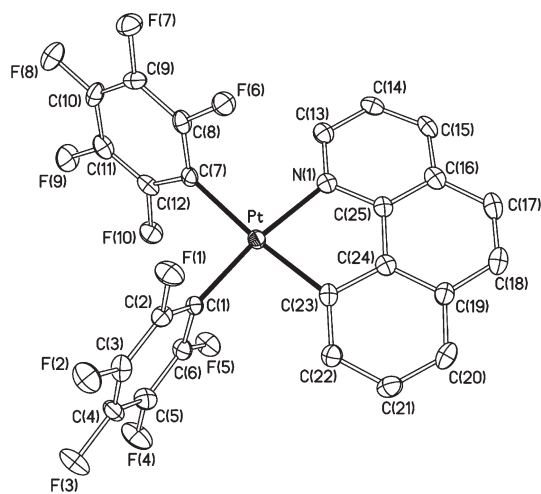


Fig. 1 View of the molecular structure of the anion of $(\text{NBu}_4)[\text{Pt}(\text{bzq})(\text{C}_6\text{F}_5)_2]$ (**1**).

Table 1 Selected bond lengths (Å) and angles (°) for $(\text{NBu}_4)[\text{Pt}(\text{bzq})(\text{C}_6\text{F}_5)_2]$ (**1**)

Pt–C(1)	2.013(4)	Pt–C(23)	2.042(4)
Pt–N(1)	2.080(3)	Pt–C(7)	2.088(4)
C(1)–Pt–C(23)	91.65(15)	C(1)–Pt–N(1)	171.83(13)
C(23)–Pt–N(1)	81.56(14)	C(1)–Pt–C(7)	92.47(15)
C(23)–Pt–C(7)	173.29(14)	N(1)–Pt–C(7)	94.73(13)

alternate. Thus, each Pt centre forms two bonds with two Ag centres, and alternatively, each silver(i) is bonded to two platinum(ii). To the best of our knowledge, there is only one similar complex formed by an infinite chain of Pt–Ag bonds, reported by Yamaguchi *et al.*²³ The Pt–Ag distances in **2** are 2.761(1) Å and 2.777(1) Å, in the range found for other complexes with η^1 -Ag–C bonds.^{13,17,23,24,34,35,38,60}

Besides the Pt–Ag bonds, the silver centre establishes a short η^1 interaction with the C_{ipso} of the bzq ligand [C(23) in Fig. 2], the distances being Ag–C(23) = 2.398(11) Å and Ag–C(23') = 2.507(11) Å. Similar η^1 -Ag–C interactions have been previously found in other cycloplatinated complexes with Pt–Ag bonds.^{17,23} These η^1 -Ag–C interactions are important and, along with the Pt–Ag bonds contribute to fulfilling the electronic requirements of the acidic silver centre and the formation of the infinite chain. We note that the affinity of silver for some aromatic π -donor systems is well known,^{33,72–77} the η^1 and η^2 coordination modes being the most usual ones. Also, the Ag–C lines are usually almost perpendicular to the plane of the aromatic rings, which is almost accomplished in complex **2** taking into consideration the additional constraints caused by the existence of the Pt–Ag bonds. Thus the angles between the Ag–C lines and the perpendicular to the best bzq planes are 11.9(6)° and 19.4(6)°. Due to the formation of the η^1 -Ag–C (bzq) contacts, the Pt–Ag bonds lean toward the bzq ligand (angles with the perpendicular 35.2(4)° and 28.1(4)°) and the silver centres move away from the bulky pentafluorophenyl groups (no *o*-F...Ag contacts are observed).

The arrangement of the sequence of bonds ...Pt–Ag–Pt–Ag... is not linear. The values of the Ag–Pt–Ag and Pt–Ag–Pt angles

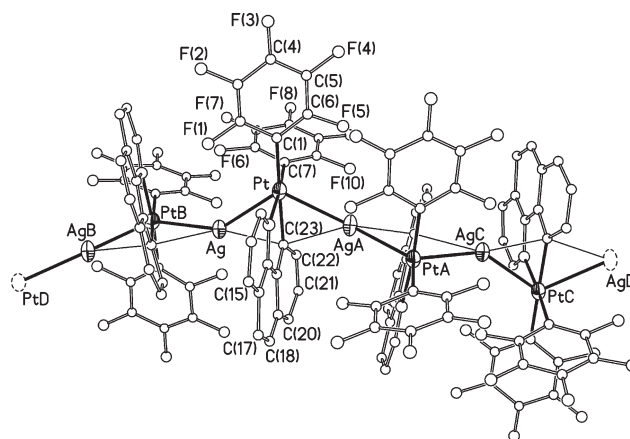


Fig. 2 View of the molecular structure of $[\{\text{Pt}(\text{bzq})(\text{C}_6\text{F}_5)_2\}\text{Ag}]_n$ (**2**).

Table 2 Selected bond lengths (Å) and angles (°) for $[\{\text{Pt}(\text{bzq})(\text{C}_6\text{F}_5)_2\}\text{Ag}]_n$ (**2**)^a

Pt–C(7)	2.028(14)	Pt–C(1)	2.065(13)
Pt–N	2.108(9)	Pt–C(23)	2.109(14)
Pt–Ag'	2.761(1)	Pt–Ag	2.777(1)
Ag–C(23)	2.398(11)	Ag–C(23'')	2.507(11)
C(7)–Pt–C(1)	87.7(5)	C(7)–Pt–N	174.7(4)
C(1)–Pt–N	95.3(4)	C(7)–Pt–C(23)	97.2(5)
C(1)–Pt–C(23)	174.4(4)	N–Pt–C(23)	80.0(4)
C(7)–Pt–Ag'	94.7(3)	C(1)–Pt–Ag'	116.9(3)
N–Pt–Ag'	87.8(3)	C(23)–Pt–Ag'	60.2(3)
C(7)–Pt–Ag	89.1(3)	C(1)–Pt–Ag	126.2(3)
N–Pt–Ag	85.6(2)	C(23)–Pt–Ag	56.8(3)
Ag'–Pt–Ag	116.9(1)	C(23)–Ag–C(23'')	144.1(4)
C(23)–Ag–Pt''	159.4(3)	C(23'')–Ag–Pt''	46.9(3)
C(23)–Ag–Pt	47.4(3)	C(23'')–Ag–Pt	135.8(3)
Pt''–Ag–Pt	145.0(1)		

^a The symmetry transformations used to generate equivalent atoms are $y - 1/4, -x + 7/4, z - 1/4$ for the primed atoms and $-y + 7/4, x + 1/4, z + 1/4$ for the double primed atoms.

are 116.9(1)° and 145.0(1)°, respectively. The dihedral angle between two consecutive Pt platinum coordination planes is 10.3(5)°. Moreover, the disposition of the ligands in the chain is such that they are rotated 90° along the main axis of the chain with respect to their positions in the preceding “Pt(bzq)(C₆F₅)₂” sub-unit, in this way configuring a helix (see Fig. 3). This is due to the fact that the chain contains a crystallographic 4₁ axis, and thus the helical motif completes every four “Pt(bzq)(C₆F₅)₂” fragments and the length of the “[Pt(bzq)(C₆F₅)₂Ag]₄” motif is 14.13 Å. Since the space group in which **2** crystallises is centrosymmetric (*I*4₁/*a*), both the right and left-handed screw helices are present in the crystal structure. A helical disposition is also observed in the Pt–Ag chain reported by Yamaguchi *et al.*,²³ but in this case the cycle of the helix comprises (PtAg)₁₂ sub-units.

The extended compound $[\{\text{Pt}(\text{bzq})(\text{C}_6\text{F}_5)_2\}\text{Ag}]_n$ (**2**) is insoluble in CH₂Cl₂, and thus, ¹H and ¹⁹F NMR spectra were recorded in acetone-*d*₆ at room temperature. The proton spectrum exhibits the expected resonances for one kind of bzq ligand and the ¹⁹F NMR spectrum exhibits two sets of C₆F₅ AA'MM'X spin systems. The equivalence of the two *o*-F and the two *m*-F on

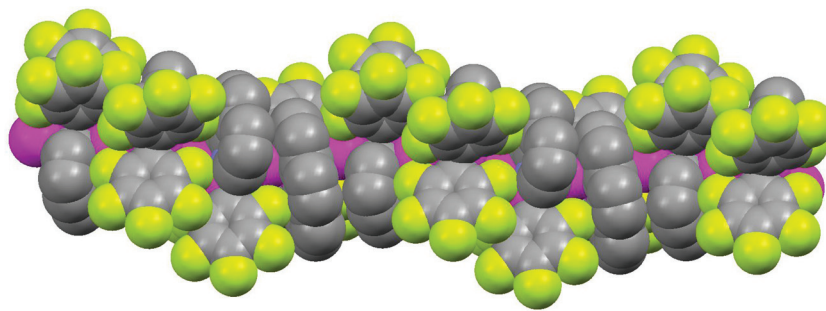


Fig. 3 View of the helical arrangement of the infinite chain in the molecular structure of $[\text{Pt}(\text{bzq})(\text{C}_6\text{F}_5)_2\text{Ag}]_n$ (**2**).

each C_6F_5 ring indicates that in acetone either the Pt–Ag bonds are cleaved or that a dynamic process (partial dissociation) is operating. The ^{195}Pt NMR spectrum was measured at two different temperatures (298 K and 253 K) showing in both cases a unique signal at -3330 and -3353 ppm respectively. These values represent a high-field shift of the signal with respect to the starting material **1** (-3705 ppm, 298 K). This, along with the low conductivity of the compound in acetone solution ($\Lambda_{\text{M}} = 37.5 \text{ } \Omega^{-1} \text{ cm}^2 \text{ mol}^{-1}$), indicates that a dynamic dissociative process is operating in acetone. Similar behaviour has been reported by Yamaguchi *et al.* for complexes $[\text{Pt}(\text{phpy})_2\text{Ag}]_x$ or $[\text{Pt}(\text{thpy})_2\text{Ag}]_x$ [$\text{Hphpy} = 2$ -phenylpyridine, $\text{Hthpy} = 2$ -(2-thyenylyl)pyridine].²³

When an equimolar amount of PPh_3 or tht (tetrahydrothiophene, SC_4H_8) is added to a suspension of **2** in CH_2Cl_2 and the mixture is stirred for 60 min, all the solid present dissolves, which seems to indicate that the cleavage of the infinite $\cdots\text{Pt}-\text{Ag}-\text{Pt}-\text{Ag}\cdots$ chain has taken place. After evaporation of the solvent and treatment of the residue (see Experimental section) the corresponding $[\{\text{Pt}(\text{bzq})(\text{C}_6\text{F}_5)_2\}\text{AgL}]$ ($\text{L} = \text{PPh}_3$ (**3**), tht (**4**)) complexes are isolated (see Scheme 1). Nevertheless, when $\text{L} = \text{py}$ only mixtures of products are obtained, of which we were only able to identify $[\text{Pt}(\text{bzq})(\text{C}_6\text{F}_5)_2\text{py}]$ (**5**) through its crystal structure, which is reported in the ESI (Fig. S1, Tables S1 and S2†). The formation of **5** indicates the occurrence of a more favourable process, involving not only the breaking of the Pt–Ag bond, but also of a Pt–C(C_6F_5) bond.

The preparation and structural characterization of $[\{\text{Pt}(\text{bzq})(\text{C}_6\text{F}_5)_2\}\text{Ag}(\text{PPh}_3)]$ (**3**) and its analogue $[\{\text{Pt}(\text{bzq})(\text{C}_6\text{Cl}_5)_2\}\text{Ag}(\text{PPh}_3)]$ had been previously carried out in our laboratory by reacting **1** (or the pentachlorophenyl analogue) with $[\text{Ag}(\text{OCIO}_3)(\text{PPh}_3)]$ in a 1 : 1 molar ratio.¹⁷ In that case, the formation of **3** involved the formation of a Pt–Ag bond. In the method described here the addition of the ligand L causes the cleavage of one of the Pt–Ag bonds on each platinum centre in the polymeric structure of **2** and the entering ligand occupies the position formerly occupied by one “Pt($\text{bzq})(\text{C}_6\text{F}_5)_2$ ” fragment. The existence of one Pt–Ag bond in **3** and **4** has been confirmed by X-ray diffraction.

We had previously reported the crystal structure of **3**,¹⁷ but more recently we have been able to obtain new crystals of this complex, which show different cell parameters from the reported ones and which correspond to a new pseudo-polymorph⁷⁸ of **3**. The relevant structural parameters of this new polymorph are very similar to those already reported in our previous paper,¹⁷ and have been only included in the ESI (Fig. S2, Tables S1 and

S3†). The existence of two polymorphs for **3** and also for the analogous silver sandwich complex $[\{\text{Pt}(\text{bzq})(\text{C}_6\text{F}_5)_2\}_2\text{Ag}]^{-17}$ seems to indicate that these kinds of “Pt(bzq)” complexes containing Pt–M dative bonds are likely to exist in different crystalline phases. Organometallic compounds are well known for their structural flexibility and it has been suggested that this molecular non-rigidity is related to the occurrence of polymorphism in the structures of these systems.⁷⁸ This flexibility has also been described in systems containing metallophilic bonds such as the trinuclear Pt–Ag–Pt complex $(\text{NBu}_4)[\{\text{Pt}(\text{C}_6\text{F}_5)_3(\text{tht})\}_2\text{Ag}]$,⁷⁹ or the heterometallic clusters $[\text{Pt}_2\text{M}_4(\text{C}\equiv\text{CR})_8]_n$ ($\text{M} = \text{Cu}$, $\text{R} = \text{Ph}$, $n = 2, 3$; $\text{M} = \text{Ag}$, $\text{R} = \text{C}_6\text{H}_4\text{-OMe}_3$, $n = 1, \infty$).^{80–82}

The crystal structure of **4** shows that, besides the tetrahydrothiophene ligand, the silver centre coordinates one acetone molecule, which is one of the solvents used to obtain suitable crystals for the X-ray study. Thus, the complex whose structure we will discuss is better formulated as $[\{\text{Pt}(\text{bzq})(\text{C}_6\text{F}_5)_2\}\text{Ag}(\text{tht})(\text{Me}_2\text{CO})]$ (**4'**). Fig. 4 shows the molecular structure of **4'** and Table 3 lists its most relevant bond distances and angles. The main feature is, as in **2** and **3**, the interaction between the $[\text{Pt}(\text{bzq})(\text{C}_6\text{F}_5)_2]$ and $[\text{Ag}(\text{tht})(\text{Me}_2\text{CO})]$ fragments through Pt–Ag (2.721(1) Å) and Ag–C(23) (2.463(3) Å) bonds. The Pt–Ag line deviates significantly ($31.4(1)^\circ$) from the perpendicular to the best Pt square plane. The Ag–S distance is 2.445(1) Å, and the Ag–O distance is 2.438(3) Å, both in the range usually found for this type of bonds.^{23,60,79,83–87} The presence of the coordinated acetone in **4'** and its absence in **3** can be explained by the different steric requirements of the ligand bonded to silver. While in **3** the bulky PPh_3 ligand “protects” the silver centre from the approximation of a further ligand, in **4'** the less sterically demanding tht allows the proximity of a small molecule such as acetone on the side of the planar bzq ligand. It is interesting to note that **4'** establishes weak $\pi\cdots\pi$ interactions in such a way that the bzq ligands of two adjacent complexes stack with an interplanar distance of *ca.* 3.5 Å (see Fig. 4b), forming dimers in a similar way to **1**, **3** or other “Pt(bzq)” complexes.^{16–18,66–71}

The ^{19}F NMR spectra of **4** both at room temperature and at 213 K in CDCl_3 show the presence of two types of C_6F_5 groups, with typical AA'MM'X spin systems. This indicates that, in the NMR time scale, the square planar Pt coordination plane is a symmetry plane. The remarkable deshielding (~ 200 ppm) observed in its $^{195}\text{Pt}\{^1\text{H}\}$ NMR spectrum in CDCl_3 at 253 K (m , -3509 ppm) and the value of the conductivity in acetone solution ($\Lambda_{\text{M}} = 22.1 \text{ } \Omega^{-1} \text{ cm}^2 \text{ mol}^{-1}$) is in accordance with a dynamic process involving partial dissociation of the Pt and Ag fragments.

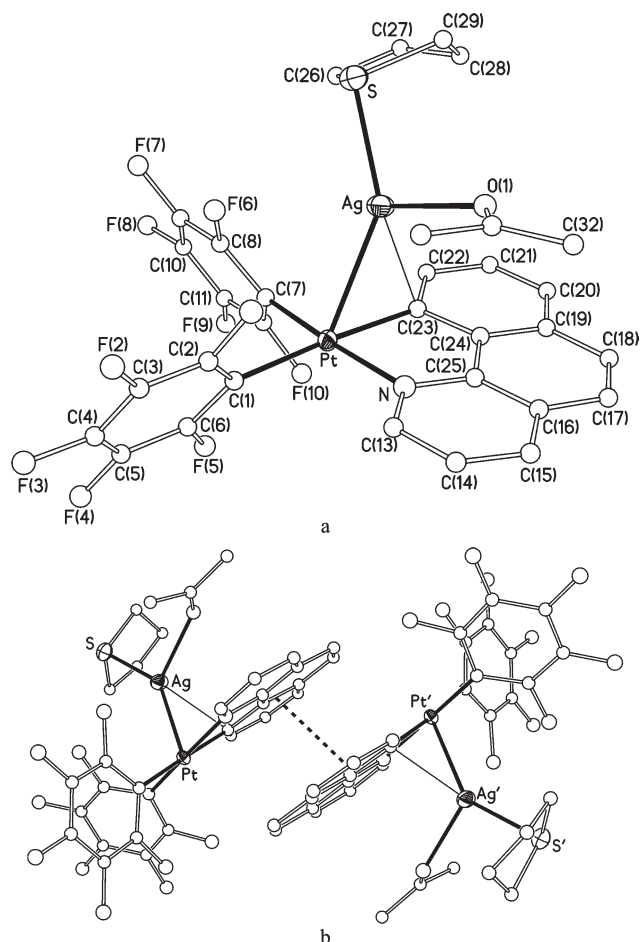


Fig. 4 a) View of the molecular structure of $[\{\text{Pt}(\text{bzq})(\text{C}_6\text{F}_5)_2\}\text{Ag}(\text{tht})(\text{Me}_2\text{CO})]$ (**4'**). b) Supramolecular arrangement in pairs of **4'**.

Table 3 Selected bond lengths (Å) and angles (°) for $[\{\text{Pt}(\text{bzq})(\text{C}_6\text{F}_5)_2\}\text{Ag}(\text{tht})(\text{Me}_2\text{CO})]\cdot\text{Me}_2\text{CO}$ (**4'**· Me_2CO)

Pt–C(7)	2.006(3)	Pt–C(23)	2.055(3)
Pt–C(1)	2.080(3)	Pt–N	2.091(3)
Pt–Ag	2.721(1)	Ag–O(1)	2.438(3)
Ag–S	2.445(1)	Ag–C(23)	2.463(3)
C(7)–Pt–C(23)	94.98(13)	C(7)–Pt–C(1)	87.88(13)
C(23)–Pt–C(1)	176.37(12)	C(7)–Pt–N	175.61(12)
C(23)–Pt–N	80.64(12)	C(1)–Pt–N	96.48(12)
O(1)–Ag–S	102.00(8)	O(1)–Ag–C(23)	97.16(11)
S–Ag–C(23)	143.10(8)	O(1)–Ag–Pt	110.09(7)
S–Ag–Pt	144.95(3)		

Electronic and luminescence spectroscopy

The absorption and emission spectra of **2** and **4** are summarized in Tables 4 and 5 and for comparative purposes some previously published data of **1** and **3** are also included. As noted before, the extended complex **2** is insoluble in CH_2Cl_2 , so that the absorption spectra were registered in THF and in acetone, in which it is assumed that the extended chain **2** dissolves as bimetallic fragments $[\{\text{Pt}(\text{bzq})(\text{C}_6\text{F}_5)_2\}\text{Ag}_n\text{S}_n]$ (S = solvent) with the donor solvent molecules completing the coordination environment of

Table 4 Absorption data (2×10^{-5} M solutions) for complexes **1–4**

Compound	Absorption/nm ($10^3 \epsilon/\text{M}^{-1} \text{cm}^{-1}$)
$(\text{NBu}_4)[\text{Pt}(\text{bzq})(\text{C}_6\text{F}_5)_2]$ (1)	243(66.4), 260(58.4), 315(27.15), 345(20.1), 380(12.1), 425(6.9) (CH_2Cl_2) ^{a,b}
$[\{\text{Pt}(\text{bzq})(\text{C}_6\text{F}_5)_2\}_2\text{Ag}]_n$ (2)	243(46.9), 262(40.3), 317(11.0), 352(8.4), 399(5.6), 448(2.5) (THF)
	215(21.0), 328(13.4), 344(12.0), 393(8.4), 422sh(5.8) (acetone) ^a
	265, 310, 357, 392, 434, 472 (solid)
	228(42.3), 254(43.8), 315(7.5), 354(4.2), 377(2.8), 419(1.5) (THF)
$[\{\text{Pt}(\text{bzq})(\text{C}_6\text{F}_5)_2\}\text{Ag}(\text{PPh}_3)]$ (3)	327(9.8), 350(7.2), 375(4.6), 418(2.3) (acetone)
	262, 314, 358, 429, 490–520 (solid)
	221sh(19.2), 239(62.0), 278sh(27.4), 311(15.9), 340(8.2), 365(4.8), 413(3.4) (CH_2Cl_2) ^b
$[\{\text{Pt}(\text{bzq})(\text{C}_6\text{F}_5)_2\}\text{Ag}(\text{tht})]$ (4)	222(57.4), 241sh(48.0), 256(42.6), 279sh(15.4), 303(10.3), 344(5.2), 389(2.6), 423(1.1) (acetonitrile) ^b
	228(42.1), 253(42.4), 293(15.2), 352(5.2), 378(3.4), 405(2.8) (CH_2Cl_2)
	229(50.4), 254(52.2), 316(13.5), 352(7.0), 378(4.9), 416(3.7) (THF)
	329(8.9), 351(5.0), 373(4.0), 408(2.5) (acetone)
	282(16.0), 315(14.4), 359(4.9), 380(3.6), 421(2.8) (toluene)
	258, 326, 360, 418, 480 (solid)

^a Values taken from ref. 16 (5×10^{-5} M). ^b Values taken from ref. 17 (5×10^{-5} M).

the silver centre. Absorption spectra of diluted solutions of the Pt–Ag complexes **2** (THF, acetone) and **4** (CH_2Cl_2 , THF, acetone, toluene) showed high-energy intraligand absorptions (range 215–373 nm) and a less intense band at 405–421 nm. With reference to previous spectroscopic work on cycloplatinate complexes and the theoretical calculations in binuclear complexes $[\{\text{Pt}(\text{bzq})(\text{C}_6\text{F}_5)_2\}\text{Ag}(\text{PPh}_3)]$ (**3**) and $[\{\text{Pt}(\text{bzq})(\text{C}_6\text{F}_5)_2\}\text{Ag}(\text{tht})(\text{acetone})]$ (**4'**) (see below), the low energy band is assigned to an admixture of metal-to-ligand $[\text{d}_\pi(\text{Pt}) \rightarrow \pi^*(\text{bzq})]$ and ligand to ligand $[\text{Ar}_\text{r} \rightarrow \text{bzq}]$ charge transfer transitions (Fig. 5). This low-energy band, which follows the Beer–Lambert law in a range of concentrations from 10^{-4} M to 10^{-5} M, is clearly blue-shifted in relation to the precursor **1** (*ie*, CH_2Cl_2 , 405 nm **4** vs. 425 nm **1**; acetone, 418 **2**, 408 nm **4** vs. 422 nm **1**; THF, 419 nm **2**, 416 nm **4** vs. 448 nm **1**), confirming the persistence of Pt–Ag bonds even in donor solvents. This observation has been previously noted in related complexes such as **3** (λ_{max} CH_2Cl_2 413 nm),¹⁷ $[(\text{N}^{\wedge}\text{N})\text{PtR}_2\text{M}](\text{OTf})$ ($\text{N}^{\wedge}\text{N} = \text{ArNC}(\text{Me})\text{C}(\text{Me})\text{NAr}$; Ar = 2,6-dichlorophenyl; M = Cu, Ag; R = Me, Ph)²⁴ or $[\{\text{Pt}(\text{bzq})(\text{C}_6\text{F}_5)_2\}\text{Cd}(\text{cyclen})]\text{ClO}_4$ (λ_{max} CH_2Cl_2 410 nm),¹⁶ in which the presence of Pt–M bond was also supported by ³¹P {¹H}, ¹H or ¹⁹F NMR spectroscopy. In these systems, the donation of electron density from Pt(d^8) to a d^{10} ion (Ag^+ or Cd^{2+}) increases the electrophilicity of the Pt centre, lowering the energy of the HOMO and, hence, increasing the gap of the ¹MLCT $[\text{5d}(\text{Pt}) \rightarrow \pi^*(\text{bzq})]$ absorption.

The solid state diffuse reflectance spectra of the extended chain **2** display a distinctive low-energy feature (490–520 nm **2**) (Fig. S3†), which is slightly blue-shifted in **4** and is absent in the

Table 5 Photophysical data for complexes **1–4** [solid state and glasses (5×10^{-5} M)]

Compound	(T/K)	λ_{em}/nm { $\Phi/\%$ }	$\tau/\mu s$
[NBu ₄][Pt(bzq)(C ₆ F ₅) ₂] (1) ¹⁷	Solid (298)	518	16.5 ^a
	Solid (77)	514, 550, 595sh	
	CH ₂ Cl ₂ (77)	485, 521, 563, 608sh ^b	
	THF (77)	485, 522, 565, 611sh ^c	
[Pt(bzq)(C ₆ F ₅) ₂] ₂ Ag _n (2)	Solid (298)	560 {6.1}	13.2
	Solid (77)	590	16.8
	THF (77)	495max, 530, 575sh	
[Pt(bzq)(C ₆ F ₅) ₂]Ag(PPh ₃) (3) ¹⁷	Solid (298)	491max, 523, 562sh {12.7}	12.4
	Solid (77)	487 ⁺ , 502 ⁺ , 585 ⁺	12.4 (487 nm) [~278(45%), ~13.6(55%)] ^d
	CH ₂ Cl ₂ (77)	495max, 530, 570, 625 sh	
[Pt(bzq)(C ₆ F ₅) ₂]Ag(tht) (4)	Solid (298)	490max, 520, 560sh {27.8}	27.9 (490)
	Solid (77)	490max, 525, 565sh	35.1 (490) [31.4(68%), 98.2(32%)] (525)
	CH ₂ Cl ₂ (77)	480max, 515, 553sh	
	THF (77)	492max, 525, 565	

^a Measured in KBr pellets at 298 K. ^b CH₂Cl₂ 5×10^{-5} M, 298 K: weak band at 520 nm, λ_{exc} 365 nm. ^c THF 5×10^{-5} M, 298 K: weak band at 525 nm, λ_{exc} 365 nm. ^d Measurements in the low energy peak.

precursor. This band is tentatively assigned to an admixture of [Pt(bzq)→Ag] (LMM'CT) and [Ar_r→Ag] (L'M'CT), involving the promotion of electron density from platinum fragments to the silver centre.

The platinum precursor **1** exhibits in solid state at room temperature a broad unsymmetrical green phosphorescence (~518 nm), also detected as a weak broad emission in CH₂Cl₂ (~520 nm) or THF (~525 nm) solutions. Upon cooling to 77 K, the spectra display a blue-shifted vibronic structured band (514 solid, 485 nm CH₂Cl₂ or THF glasses), which according to theoretical calculations, is mainly ascribed to an admixture of ³[$\pi \rightarrow \pi^*(bzq)$] (³LC) and ³[5d(Pt)→ $\pi^*(bzq)$] (³MLCT) triplet excited states (Fig. 6a, solid state).

Complexes **2–4** were only emissive in rigid media (solid and glasses) (see Table 5). The lack of luminescence in solution could be attributed to the decreasing contribution of ³MLCT to the excited state (see below). For comparative purposes, the emission spectra of the precursor **1** and **4** are shown in Fig. 6. As is shown in Fig. 6b, upon formation of the Pt–Ag bond, the emission of **4** in solid state at 298 K becomes structured with a λ_{max} hypsochromically shifted (λ_{max} 490 nm, $\Phi = 27.8\%$, 298 K, 77 K) in relation to the precursor, thus reflecting the stabilization of the HOMO level. The clear vibronic appearance of the emission at 298 K as well as the lack of rigidochromism and the increasing of the lifetime on going to 77 K ($\tau = 27.9 \mu s$,

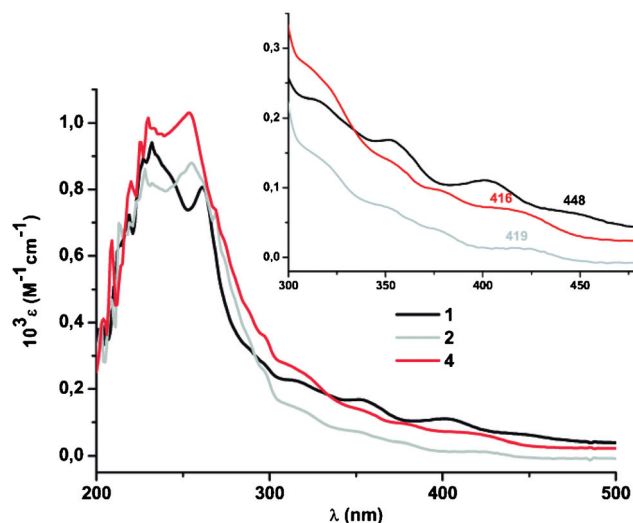


Fig. 5 Absorption spectra of **1**, **2** and **4** in THF, 2×10^{-5} M at 298 K. Inset: low-energy region.

298 K; 35.1 μs , 77 K) in relation to **1**, suggest that the contribution of the ³MLCT to the emissive state decreases on going from **1** to **4**. This hypothesis is consistent with the fact that the formation of the Pt–Ag dative bond increases the electrophilicity of the Pt centre, raising the energy of the ³MLCT. While the lifetime at the peak maxima fits to one component, at 77 K the decay in the shoulder is composed of two components [$\tau = 31.4$ (68%), 98.2 (32%) μs , (525 nm)], which indicates that the emission still has some degree of mixed origin. Curiously, the behaviour of **4** in the solid state contrasts with that of the related PPh₃ derivative **3**. In this complex **3**, the vibronic band with a λ_{max} 491 nm ($\Phi = 12.7\%$, $\tau = 12.4 \mu s$) seen at 298 K is clearly resolved at 77 K into two close non-equilibrated structured bands with different origins (487 and 502 nm, respectively) and also distinct decays (see Table 5), which were tentatively ascribed in our previous work to ³MLCT (or a mixed ³LC/³MLCT) manifold.¹⁷ In this work, the nature of the low-lying phosphorescent emission has been addressed by DFT calculations. Inspection of the salient features of the SOMOs in the optimized T₁ state for both complexes (see Theoretical section) suggests that the emissions are mainly associated with charge transfer from the metals and C₆F₅ groups to the low lying benzoquinolate group with some intraligand (bzq) character. Due to the low contribution of the Ag to the SOMO (3% in **3** and 4% in **4**) we suggest that the emission comes mainly from an admixture of ³MLCT/³L/LCT.

It is worth noting that despite the presence of short $\pi \cdots \pi$ contacts between the bzq ligands of two adjacent monomers in complexes **1**, **3** and **4** (~3.6 Å in **1**, 3.4–3.5 Å in **3** and **4**), leading to final $\pi \cdots \pi$ stacked dimers, these interactions are not reflected in the energy of their emissions, probably because they are not of a long-range. By contrast, the presence of an extended metallic [–Pt–Ag–Pt–Ag–] chain in complex **2** is reflected in its optical behaviour. In solid state, **2** exhibits a bright ($\Phi = 6.1\%$) orange emission (560 nm) with a mono exponential decay of 13.2 μs , revealing its triplet parentage. The emission is remarkably red-shifted in relation to the precursor (**1**, 518 nm) and also

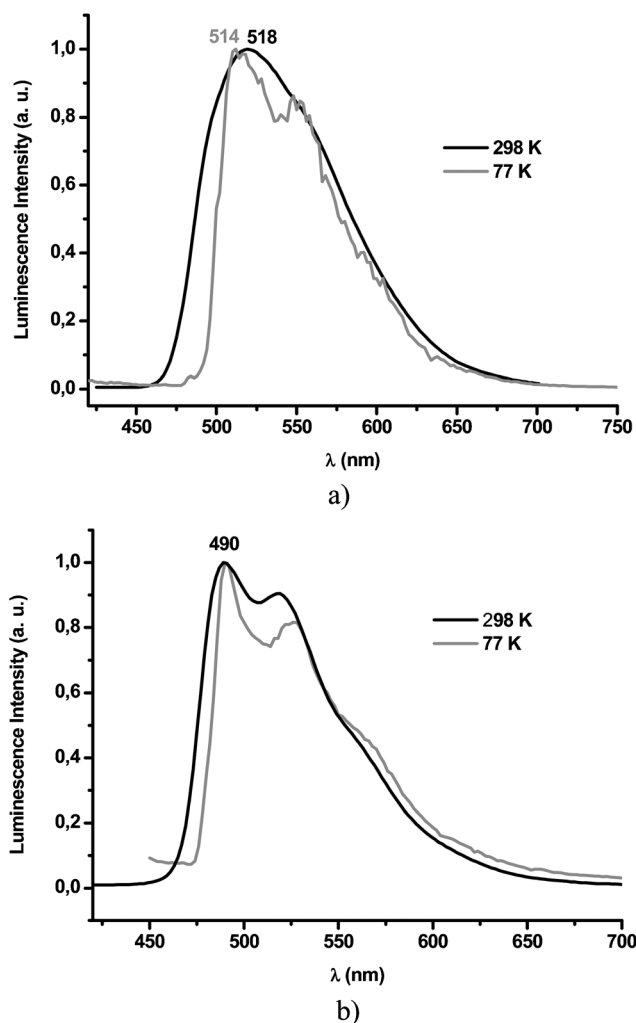


Fig. 6 Normalized emission spectra of **1** (a) and **4** (b) in solid state at 298 K and at 77 K (λ_{exc} 400 nm).

upon cooling at 77 K (590 nm **2**) pointing to the involvement of Pt–Ag bonds and Ag orbitals in the excited state (Fig. 7). The excitation profile with a low-energy peak at \sim 500 nm mimics the solid reflectance diffuse spectrum (see Fig. S3[†]). According to the contributions of the metals and ligands to the frontier orbitals in the bimetallic fragment “[Pt(bzq)(C₆F₅)₂Ag]” as model for **2**, we tentatively assign this emission to as arising from a mixed ³LMM⁺CT [Pt(bzq)→Ag]/³L⁺M⁺CT [Ar_f→Ag] excited state involving charge transfer from the platinum fragment to the silver centre. The presence of an extended metallic chain stabilized by the occurrence of both Pt–Ag and metallated carbon–silver [C_π(bzq)→Ag⁺] bonding interactions could raise and lower the energies of the frontier orbitals HOMO and LUMO respectively.

Not surprisingly, complex **2** dissolves in THF giving non-emissive pale-yellow solutions, probably formed by bimetallic solvated fragments [Pt(bzq)(C₆F₅)₂Ag(THF)_n]. The spectra of all three complexes **2–4** recorded in glassy (77 K) solution (**2**, THF; **3**, CH₂Cl₂; **4**, CH₂Cl₂, THF) display vibronic structures with minor variations in their maxima, suggesting luminescence from states exhibiting a primarily ³LC character.

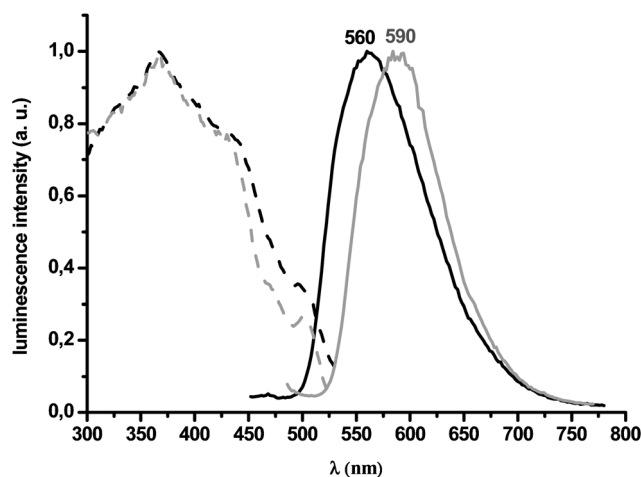


Fig. 7 Normalized excitation and emission spectra of **2** in solid state at 298 K (black) and at 77 K (grey) λ_{exc} 400 nm.

Theoretical calculations

The absorption and emission spectra of complexes **1–3** and **4'** were examined on the optimized geometries (for the S₀ and T₁ states) at the PBE1PBE/Def2-TZVP(M)U6-31+G(d,p)(X) (M = metal atom, X = non metal element) level in the gas phase. The equilibrium geometries along with selected structural parameters are shown in Fig. S4[†]. The optimized structural parameters of **1–3** and **4'**, in their S₀ ground state, closely resemble the X-ray structural analysis data. The higher deviation from the experimental value of the Pt–Ag bond length in **2** (elongated by 0.125 Å) could be due to the fact that the computed structural parameter refers to an isolated building block of the polymeric structure.

The absorption spectra of **1–3** and **4'** simulated with TD-DFT calculations in the gas phase are depicted schematically in Fig. 8. Selected TD-DFT singlet–singlet electronic transitions, excitation energies and oscillator strengths are compiled in Tables S4 and S5 (ESI[†]). Assignments on the electronic transitions, which are based on the nature of the molecular orbitals (Fig. S5–S8[†]) and electron density difference maps (EDDM) (Fig. S9[†]) are summarized in Tables S6–S9[†].

According to the shapes of the MOs involved in the transitions (Fig. 9) as well as the respective EDDM (Fig. S9[†]) and %CT values (Table S4[†]), the high energy bands for the anionic precursor **1** (245–307 nm) possess a complex set of electronic transitions (LC/L⁺LCT/MLCT; L = bzq, L⁺ = Ar_f; Ar_f = C₆F₅), while the low intensity bands in the range of 330–406 nm are mainly due to Pt→bzq and Ar_f→bzq charge transfer (MLCT/L⁺LCT). The low energy band calculated at 436 nm arises mainly from the HOMO→LUMO (84%) excitation with the HOMO constructed from the out-of-phase combination of Pt(5d_{yz}) (43%), bzq (46%) and Ar_f ligands (11%) and the LUMO located on the bzq having therefore a remarkable MLCT character.

For discrete complexes **3** and **4'** having the cationic units Ag (PPh₃) and Ag(tht)(acetone), respectively, coordinated to the anionic fragment **1** through a Pt–Ag bond, the frontier orbitals (FMOs) are quite similar (Fig. 9). Thus, in both complexes the HOMO–3 to HOMO are mainly composed of platinum AOs overlapping with MOs located on both ligands (bzq, Ar_f) with a

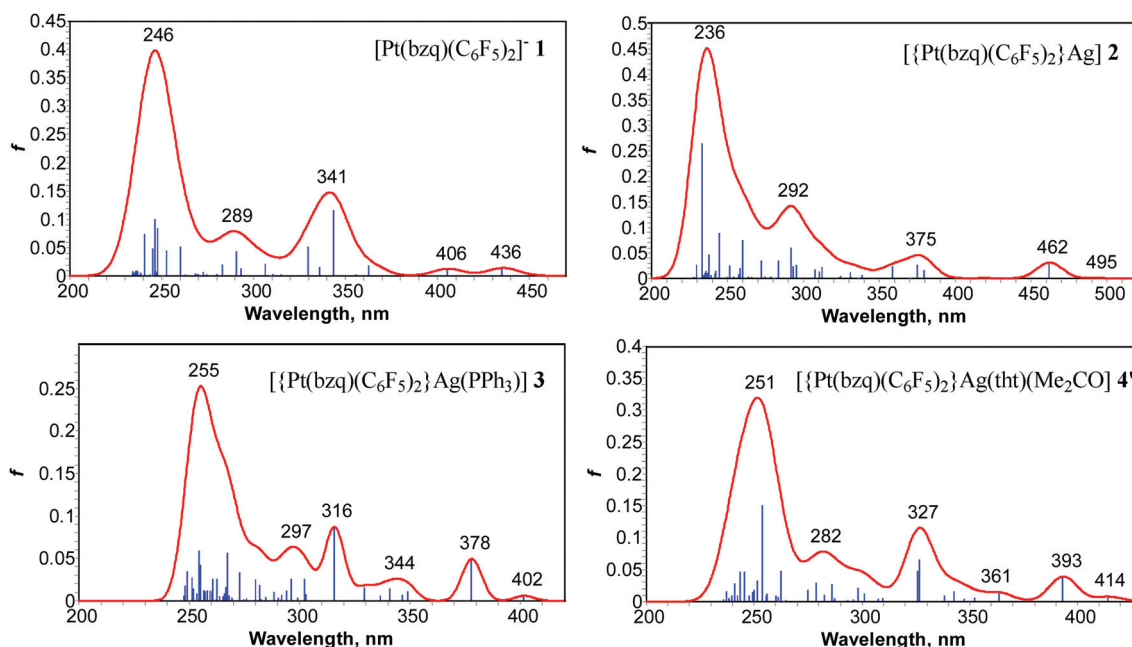


Fig. 8 TD-DFT/PBE1PBE/Def2-TZVP(M)U6-31+G(d,p)(X) simulated absorption spectra of complexes 1–3 and 4' in gas phase.

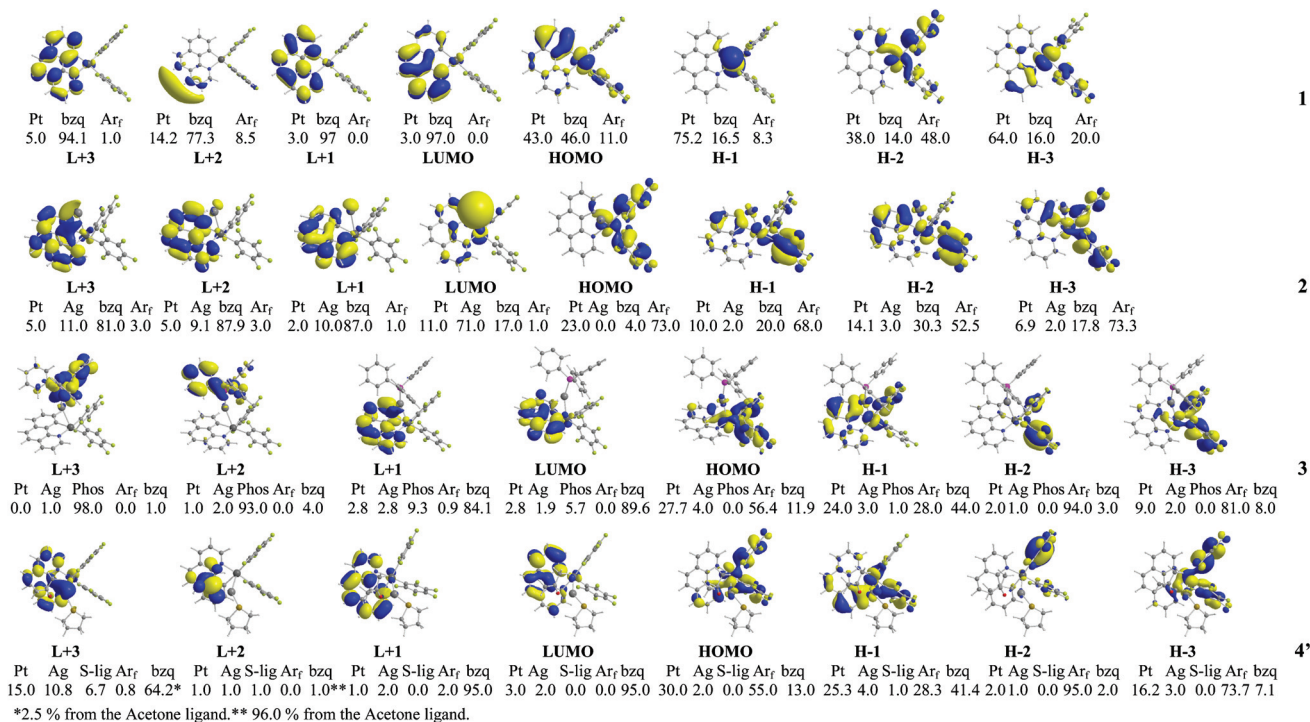


Fig. 9 Frontier molecular orbital plots for 1–3 and 4' along with their composition (%) in terms of ligands and metals obtained by DFT.

higher contribution from the MOs located on the Ar_F groups and just a marginal contribution of the AOs of Ag atom and the LUMO and LUMO+1 correspond to π* MOs located on the bzq ligand. However, while in 4 the LUMO+3 has bzq (~64%) and a metallic character (Pt 15%, Ag ~11%) with a small contribution of the tht ligand (6.7%), in complex 3 it has an essentially high (93%) orbital character from the PPh₃ ligand. Therefore, for these complexes the main difference with the precursor 1 upon

forming the Pt–Ag bond is the stabilization of the HOMO decreasing the weight of the bzq (12–13% vs. 46% in 1) and the Pt (~28% 3, 30% 4' vs. 43% in 1) orbitals and increasing the orbital character of the electron-withdrawing C₆F₅ groups (~55% vs. 11% in 1). For both complexes, the two low-energy absorptions (378, 402 nm 3; 393, 414 nm 4') are primarily associated with HOMO, HOMO–1 → LUMO transitions, showing significant %CT values (see Table S5†) and are hence

ascribed to admixture MLCT/L'LCT (L = bzq; L' = Ar_f). The calculated values are comparable to the experimental values (365, 413 nm CH₂Cl₂ **3**; 373, 408 nm acetone **4**) and are blue-shifted in relation to **1** (calculated 406, 436 nm) in agreement with the experimental results. The remaining high-energy bands (240–360 nm **3**, with peak maxima at 255, 297, 316 and 344 nm; 220–360 nm **4'**, with peak maxima at 251, 282, 327 and 361 nm) arise from a multitude of excitations (electron density difference maps and a detailed assignment of these latter electronic transitions are shown in Fig. S9† and Table S5†).

Calculations on the monomeric building block [$\{\text{Pt}(\text{bzq})(\text{C}_6\text{F}_5)_2\}\text{Ag}\}_n$ in **2** were performed as an adequate model for the polymer **2**. As can be seen in Fig. 9, Fig. S6† and Table S7,† the formation of the Pt–Ag bond has a remarkable effect in the nature of the frontier orbitals. Thus, the HOMO is mainly localized on the Pt (23%) and C₆F₅ groups (73%) and the HOMO–1 and HOMO–2 also have a significant contribution from the Ar_f groups, while the LUMO is located on the Ag metal (71%) and has a small contribution from orbitals of Pt (11%) and bzq (17%). The calculated spectrum in gas phase (Fig. 8) shows an intense band at 236 nm and several bands of medium intensity (270–350 nm), which are mainly ascribed to mixed LC/L'LCT/MLCT character with some L'M'CT (Ar_f→Ag) (see Table S4 for assignments†). The low-energy region 350–500 nm has two peak maxima at 375 nm and 462 nm and a very low band ($f = 0.0007$) at 495 nm. These bands are primarily associated with transitions to the LUMO, which is mainly located on the Ag atom: 375.4, HOMO–6 → LUMO (81%) and 380 nm, HOMO–5 → LUMO (84%); 462.2 nm, HOMO–2, HOMO–1 → LUMO (82%); 495 nm HOMO–1 → LUMO (95%). The HOMO–6 and HOMO–5 are constructed from AOs of the Pt and MOs located on the bzq ligand and therefore the band at 375 nm could be assigned as LMM'CT. However, the HOMO–2 to HOMO have a remarkable contribution from Pt and the Ar_f ligands (52.5–73%) and the bands at 462 and 495 nm also exhibit a remarkable L'M'CT character. In agreement with this, the diffuse reflectance spectrum of the solid extended chain **2** exhibits a low energy feature from 490–520 nm (Fig. S3†), which could tentatively be ascribed as an admixture of [Pt(bzq)→Ag] (LMM'CT) and [Ar_f→Ag] (L'M'CT) involving charge transfer from the platinum fragments to the silver centres.

However, as it has been noted before, in acetone or THF solution complex **2** dissolves giving discrete bimetallic fragments [$\{\text{Pt}(\text{bzq})(\text{C}_6\text{F}_5)_2\}\text{AgS}_n$] (S = solvent) analogous to [$\{\text{Pt}(\text{bzq})(\text{C}_6\text{F}_5)_2\}\text{AgL}$] (L = PPh₃ **3**, tht **4**). Therefore, for complex **2** in solution the low energy bands are assigned, as in **3** and **4**, to admixture MLCT/L'LCT.

The lowest-energy emissions for complexes **1–3** and **4'**, calculated as $\Delta E_{T_1-S_0}$, occur at 554.2, 563.8, 484.9 and 467.5 nm respectively, closely resembling with the experimentally observed emission bands with maxima at 518, 560, 491 and 490 nm in the solid state emission spectra of **1–4** respectively. The phosphorescent emission of **1–3** and **4'** can be associated with the singly occupied molecular orbitals (SOMO) and SOMO–1 of the optimized T₁ state. The 3D contour plots of the SOMO and SOMO–1 of complexes **1–3** and **4'** and their composition (%) in terms of ligands and metals are shown in Fig. 10. For complex **1**, the SOMO–1 is mainly contributed from bzq (81.2%) and Pt (16.8%) centre, whereas the SOMO is located on the bzq (99%), pointing to a ligand-centred (bzq) ³LC character mixed with ³MLCT contribution. For the bimetallic complexes **3** and **4'**, the SOMO–1 resembles the HOMO of the ground state, with contribution of Pt (24.2% **3**, 29.3% **4'**) and both ligands (bzq, Ar_f) with a marginal contribution of the silver, whereas the SOMO is located on the bzq. Therefore, their emissions could be primarily ascribed to a ³MLCT/³L'LCT manifold. For model **2**, given that the SOMO is located in both metals (Pt 16.8%, Ag 64%) whereas the SOMO–1 is distributed over the platinum fragment with a remarkable contribution of the Ar_f rings (52.5%), the emission can be assigned as an admixture of [Pt(bzq)→Ag] (³LMM'CT) and Ar_f→Ag (³L'M'CT).

Conclusions

To summarize, an unusual polymer metallic chain system [$\{\text{Pt}(\text{bzq})(\text{C}_6\text{F}_5)_2\}\text{Ag}\}_n$ (**2**) and a series of bimetallic [$\{\text{Pt}(\text{bzq})(\text{C}_6\text{F}_5)_2\}\text{AgL}$] complexes (**3**, **4**) stabilized by short Pt–Ag (2.75 Å) and $\eta^1 \text{Ag}\cdots\text{C}(\text{bzq})$ (~2.45 Å) bonding interactions have been constructed starting from the anionic [Pt(bzq)(C₆F₅)₂][–] (**1**) building block. Their photophysical properties (absorption and emission) have been studied and discussed with theoretical calculations to obtain greater insight into the

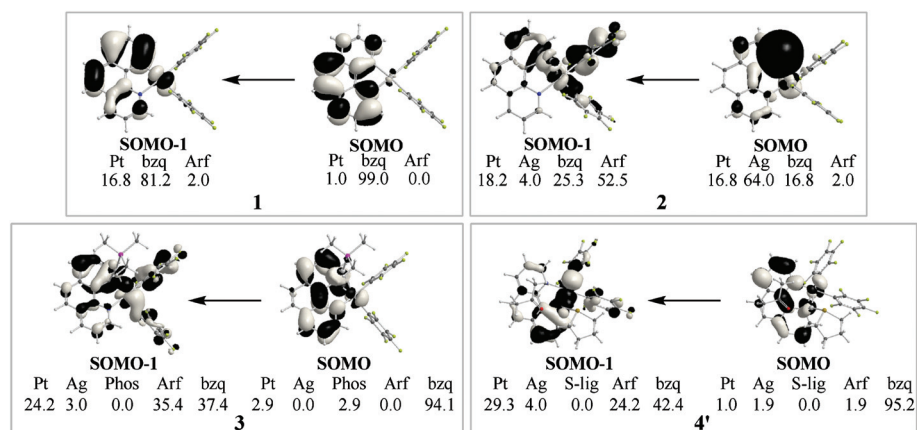


Fig. 10 3D contour plots of SOMO and SOMO–1 for **1–3** and **4'** involved in the emission process along with their composition (%) in terms of ligands and metals obtained by DFT.

influence of d^8-d^{10} metallophilic bonds on the nature of the electronic transitions.

For complexes **3** and **4** (and also for **2** upon solution in donor solvents as acetone or THF) the formation of the Pt–Ag bond produces a significant blue shift of the lowest-lying absorption in relation to **1**. This fact has been attributed to the stabilization and modification of the nature of the HOMO, which changes the character of the transition from ${}^1\text{LC}/{}^1\text{MLCT}$ in **1** to admixture ${}^1\text{L}/\text{LCT}/{}^1\text{MLCT}$ with a lower weight of the ${}^1\text{MLCT}$ in the bimetallic fragments. The emission in **3** and **4** is also mainly associated with an admixture of ${}^3\text{MLCT}/{}^3\text{L}/\text{LCT}$, only slightly modified by the Ag centre. By contrast, both the experimental data in solid state and the theoretical calculations on “[Pt(bzq)(C₆F₅)₂]Ag” as the model for **2** suggest that excitation of the polymer moves electron density from the platinum fragments, the C₆F₅ rings having a remarkable contribution to an orbital with a strong Pt, Ag metallic character. Absorption and emission of the polymer in the solid state is therefore suggested to be associated with an electronic transition of a mixed [Pt(bzq)→Ag]/[Ar₁→Ag] character.

Experimental

General comments

Literature methods were used to prepare the starting material (NBu₄)[Pt(bzq)(C₆F₅)₂] (**1**).¹⁶ C, H and N analyses, mass, conductivity, IR and NMR spectra were performed as described elsewhere.¹⁶ Diffuse reflectance UV-vis (DRUV) data of pressed powder were recorded on a Shimadzu UV-3600 spectrophotometer with a Harrick Praying Mantis accessory and recalculated following the Kubelka–Munk function. The optical absorption spectra were recorded using a Hewlett Packard 8453 (solution) spectrophotometer in the visible and near-UV ranges. Emission and excitation spectra were obtained on a Jobin-Yvon Horiba Fluorolog 3-11 Tau-3 spectrofluorimeter and the lifetimes were measured operating in the phosphorimeter mode with a F1-1029 lifetime emission PMT assembly, using a 450 W Xe lamp. Quantum yields in the solid state were measured upon excitation at 400 nm, using an F-3018 Integrating Sphere mounted on a Fluorolog 3-11 Tau-3 spectrofluorimeter.

Safety note: Perchlorate salts of metal complexes with organic ligands are potentially explosive. Only small amounts of material should be prepared and these should be handled with great caution.

Preparation of [Pt(bzq)(C₆F₅)₂]Ag_n (**2**)

To a solution of AgClO₄ (0.069 g, 0.336 mmol) in acetone (15 mL), (NBu₄)[Pt(bzq)(C₆F₅)₂] **1** (0.319 g, 0.336 mmol) was added. After 1 h of stirring in absence of light the solution was evaporated to dryness. CH₂Cl₂ (5 mL) was added and **2** crystallized. The yellow solid was filtered off, washed with cold CH₂Cl₂ (3 × 1 mL) and vacuum-dried, 0.209 g, 76% yield. Anal. Found (calcd for C₂₅H₈AgF₁₀NPt): C, 36.42 (36.81); H, 0.85 (0.99); N, 1.83 (1.79). IR (cm⁻¹): 1634 (w), 1507 (s), 1061 (s), 954 (s), 835 (s), 819 (w), 802 (s), 784 (m, C₆F₅, X-sensitive vibr.),⁸⁸ 766 (m, C₆F₅, X-sensitive vibr.).⁸⁸ A_M (acetone) = 37.5 Ω⁻¹ cm² mol⁻¹. ¹H NMR (acetone-d₆, 295 K), δ 8.6 (H₄, dd,

³J_{H(4),H(3)} = 8.0 Hz, ³J_{H(4),H(2)} = 0.8 Hz), 8.4 (H₂, d, ³J_{H(2),H(3)} = 5.2 Hz, ³J_{H(2),Pt} = 28 Hz), 7.7 (H₅, d, ³J_{H(5),H(6)} = 8.8 Hz), 7.6 (H₃, dd, ³J_{H(3),H(4)} = 8.0 Hz, ³J_{H(3),H(2)} = 5.2 Hz), 7.6 (H₆, d, ³J_{H(6),H(5)} = 8.8 Hz), 7.5 (H₇, dd, ³J_{H(7),H(8)} = 8.0 Hz, ³J_{H(7),H(9)} = 0.8 Hz), 7.2 (H₈, dd, ³J_{H(8),H(7)} = 8.0 Hz, ³J_{H(8),H(9)} = 6.0 Hz), 7.2 (H₉, dd, ³J_{H(9),H(8)} = 6.0 Hz, ³J_{H(9),H(7)} = 0.8 Hz, ³J_{H(9),Pt} = 34 Hz). ¹⁹F NMR (acetone-d₆, 295 K), δ -114.1 (o-F, d, ³J_{F,F} = 28 Hz, ³J_{F,Pt} = 552 Hz), -117.0 (o-F, d, ³J_{F,F} = 28 Hz, ³J_{F,Pt} = 320 Hz), -165.2 (p-F, t, ³J_{F,F} = 20 Hz), -165.7 (m-F, br m), -166.5 (p-F, t, ³J_{F,F} = 20 Hz), -166.7 (m-F, br m). ¹⁹F NMR (acetone-d₆, 183 K), δ -113.8 (o-F, br s, ³J_{F,Pt} = 426 Hz), -117.0 (o-F, br s, ³J_{F,Pt} = 207 Hz), -164.4 (p-F, t, ³J_{F,F} = 30 Hz), -164.9 (m-F, br m), -165.6 (p-F, t, ³J_{F,F} = 30 Hz), -165.9 (m-F, br m). ¹⁹⁵Pt{¹H} NMR (acetone-d₆, 295 K), δ -3330 [Pt, m]; (acetone-d₆, 253 K), δ -3353 [Pt, m].

Preparation of [Pt(bzq)(C₆F₅)₂]Ag(PPh₃) (**3**)

This complex has now been obtained by a different method to that previously reported.¹⁷ To a yellow suspension of **2** (0.100 g, 0.123 mmol) in CH₂Cl₂ (10 mL), PPh₃ was added (0.032 g, 0.123 mmol). After 30 min of stirring in absence of light, the solution was evaporated to dryness. The residue was treated with *n*-hexane, filtered off and finally air-dried, 0.104 g, 79% yield. Anal. Found (calcd for C₄₃H₂₃AgF₁₀NPt), C 47.66 (47.91); H 2.26 (2.15); N 1.37 (1.30). IR (Nujol): IR (cm⁻¹): 1632 (w), 1500 (s), 1098 (m), 1060 (s), 1044 (m), 955 (s), 836 (m), 821 (w), 801 (m, C₆F₅, X-sensitive vibr.),⁸⁸ 777 (m, C₆F₅, X-sensitive vibr.),⁸⁸ 742 (s), 692 (s), 522 (m), 505 (m). IR and ¹H, ¹⁹F and ³¹P{¹H} NMR agree with those described in ref. 17. ¹⁹⁵Pt{¹H} NMR (CDCl₃, 233 K), δ -3507 [Pt, m].

Preparation of [Pt(bzq)(C₆F₅)₂]Ag(tht) (**4**)

To a yellow suspension of **2** (0.242 g, 0.297 mmol) in CH₂Cl₂ (5 mL), tht was added (26.2 μL, 0.297 mmol). After 1 h of stirring in absence of light the solution was evaporated to dryness. The residue was treated with ether, filtered off and finally air-dried, 0.181 g, 68% yield. Anal. Found (calcd for C₂₉H₁₆AgF₁₀NPtS), C 38.11 (38.54); H 1.15 (1.79); N 1.65 (1.55); S 3.43 (3.56). IR (cm⁻¹): 1630 (w), 955 (s), 884 (s, tht), 835 (m), 819 (w), 799 (m, C₆F₅, X-sensitive vibr.),⁸⁸ 777 (m, C₆F₅, X-sensitive vibr.),⁸⁸ 756 (s), 672 (s), 620 (s), 515 (m). A_M (acetone) = 22.2 Ω⁻¹ cm² mol⁻¹. ¹H NMR (CDCl₃, 295 K), δ 8.6 (H₂, d, ³J_{H(2),H(3)} = 4.8 Hz, ³J_{H(2),Pt} = 31 Hz), 8.3 (H₄, d, ³J_{H(4),H(3)} = 7.8 Hz), 7.7 (2 H, m), 7.6 (H₆, d, ³J_{H(6),H(5)} = 9.0 Hz), 7.4 (3 H, m), 3.0 (tht, s); 2.0 (tht, s). ¹⁹F NMR (CDCl₃, 295 K), δ -115.5 (o-F, d, ³J_{F,F} = 28 Hz, ³J_{F,Pt} = 539 Hz), -118.5 (o-F, d, ³J_{F,F} = 28 Hz, ³J_{F,Pt} = 330 Hz), -162.4 (p-F, t, ³J_{F,F} = 20 Hz), -163.6 (m-F+ p-F, br m), -164.6 (m-F, br m). ¹⁹F NMR (CDCl₃, 213 K), δ -115.5 (o-F, d, ³J_{F,F} = 19 Hz, ³J_{F,Pt} = 540 Hz), -118.4 (o-F, d, ³J_{F,F} = 28 Hz, ³J_{F,Pt} = 327 Hz), -162.1 (p-F, br s, ³J_{F,F} = 20 Hz), -163.2 (m-F+ p-F, br m), -164.0 (m-F, br m). ¹⁹⁵Pt{¹H} NMR (CDCl₃, 253 K), δ -3509 [Pt, m].

Reaction of [Pt(bzq)(C₆F₅)₂]Ag_n (**2**) with py

To a yellow suspension of **2** (0.100 g, 0.123 mmol) in CH₂Cl₂ (5 mL), pyridine was added (10 μL, 0.123 mmol). After 1 h of

stirring in absence of light the solution was evaporated to dryness. The residue was treated with ether, filtered off and finally air-dried (0.072 g). The solid is a mixture of complexes, one of which was identified (X-ray) as [Pt(bzq)(C₆F₅)(py)] (5).

X-ray structure determinations

Crystal data and other details of the structure analyses are presented in Table 6 (full data for the X-ray analyses of **3** and **5** are presented in the ESI, Table S1†). Suitable crystals for X-ray diffraction studies were obtained by slow diffusion of *n*-hexane into concentrated solutions of the complexes in 3 mL of Me₂CO. Crystals were mounted at the end of a quartz fibre. The radiation used in all cases was graphite monochromated MoK α (λ = 0.71073 Å). For 4'-Me₂CO, X-ray intensity data were collected on a Bruker Smart Apex diffractometer. The diffraction frames were integrated using the SAINT program⁸⁹ and the reflections corrected from absorption with SADABS.⁹⁰ For the rest of the structures, X-ray intensity data were collected on an Oxford Diffraction Xcalibur diffractometer. The diffraction frames were integrated and corrected from absorption by using the CrysAlis RED program.⁹¹ The structures were solved by Patterson and Fourier methods and refined by full-matrix least squares on F^2 with SHELXL-97.⁹² All non-hydrogen atoms were assigned anisotropic displacement parameters and refined without positional constraints, except as noted below. All hydrogen atoms were constrained to idealized geometries and assigned isotropic displacement parameters equal to 1.2 times the U_{iso} values of their attached parent atoms (1.5 times for the methyl hydrogen atoms). Full-matrix least-squares refinement of these models against F^2 converged to final residual indices given in Table 6.

Computational details

The geometries of all stationary points were fully optimized, without symmetry constraints, employing the 1997 hybrid functional of Perdew, Burke and Ernzerhof⁹³ as implemented in the Gaussian03 program suite.⁹⁴ This functional uses 25% exchange and 75% correlation weighting and is denoted as PBE0. For the geometry optimizations we have used the Def2-TZVP basis set for Pt and Ag metal atoms and the 6-31+G(d,p) for all other non metal atoms. Hereafter the method used in DFT calculations is abbreviated as PBE0/Def2-TZVP(M)6-31+G(d,p)(X) (M = metal atom, X = non-metal element). All stationary points have been identified as minima (number of imaginary frequencies NImag = 0).

Gas-phase time-dependent DFT (TD-DFT) calculations of the lowest 50 singlet–singlet excitations were performed at the PBE0/Def2-TZVP(M)6-31+G(d,p)(X) level, using the S₀ ground state geometries of complexes **1–3** and **4'** as obtained from the optimizations at the same level of theory in order to simulate the absorption spectra of these species. The unrestricted uPBE0 was used to optimize the lowest triplet state (T₁) for complexes **1–3** and **4'** for the investigation of the nature of the emissive state. The calculated emission maxima were estimated from the differences between the triplet- and ground-state energies at their corresponding equilibrium geometries. All TD-DFT calculations were performed using the Gaussian03 suite of programs.⁹⁴

Acknowledgements

This work was supported by the Spanish MICINN (DGPTC/FEDER) (Project CTQ2008-06669-C02-01,02/BQU). S. Ibáñez

Table 6 Crystal data and structure refinement for complexes [NBu₄][Pt(bzq)(C₆F₅)₂] (**1**), [{Pt(bzq)(C₆F₅)₂}Ag]_n (**2**), and [{Pt(bzq)(C₆F₅)₂}Ag(tht)(Me₂CO)]·Me₂CO (**4'**·Me₂CO)

	1	2	4' ·Me ₂ CO
Formula	C ₄₁ H ₄₄ F ₁₀ N ₂ Pt	(C ₂₅ H ₈ AgF ₁₀ NPt) _n	C ₃₃ H ₂₂ AgF ₁₀ NOPtS·Me ₂ CO
M_r	949.87	815.28	1019.60
Crystal system	Triclinic	Tetragonal	Triclinic
Space group	$P\bar{1}$	$I4_1/a$	$P\bar{1}$
$a/\text{Å}$	9.8757(3)	25.8768(3)	11.0879(14)
$b/\text{Å}$	11.6449(3)	25.8768(3)	12.7152(17)
$c/\text{Å}$	18.5109(5)	18.5465(2)	13.3809(18)
$\alpha/^\circ$	100.069(2)	90	80.369(2)
$\beta/^\circ$	98.845(2)	90	76.834(2)
$\gamma/^\circ$	114.516(2)	90	68.048(2)
$V/\text{Å}^3$	1845.17(9)	12418.9(3)	1696.7(4)
Z	2	16	2
$D_c/\text{g cm}^{-3}$	1.710	1.744	1.996
T/K	100(1)	123(1)	100(1)
μ/mm^{-1}	3.886	5.203	3.658
$F(000)$	944	6080	984
2θ range/ $^\circ$	7.4–50.0	8.3–51.0	3.2–50.0
Collected reflections	19190	39290	9235
Unique reflections	6451	5732	5887
R_{int}	0.0276	0.0656	0.0124
R_1, wR_2^a ($I > 2\sigma(I)$)	0.0262, 0.0675	0.0556, 0.1481	0.0215, 0.0535
R_1, wR_2^a (all data)	0.0312, 0.0688	0.0871, 0.1546	0.0225, 0.0540
GOF (F^2) ^b	1.076	1.006	1.041

^a $R_1 = \sum(|F_o| - |F_c|) / \sum |F_o|$, $wR_2 = [\sum w(F_o^2 - F_c^2)^2 / \sum w(F_o^2)^2]^{1/2}$. ^b Goodness-of-fit = $[\sum w(F_o^2 - F_c^2)^2 / (n_{\text{obs}} - n_{\text{param}})]^{1/2}$.

thanks the Ministerio de Educación y Ciencia for a grant. A. C. T. thanks the University of Ioannina for a sabbatical leave and all colleagues at the Departamento de Química Inorgánica, Instituto de Ciencia de Materiales de Aragón, Facultad de Ciencias, Universidad de Zaragoza-CSIC, Zaragoza (Spain) for their generous hospitality. In particular I want to single out my host Professor Juan Forniés for his hospitality and support during this sabbatical leave.

References

- P. Pyykkö, *Chem. Rev.*, 1997, **97**, 597.
- P. Pyykkö, *Angew. Chem., Int. Ed.*, 2004, **43**, 4412.
- L. H. Gade, *Angew. Chem., Int. Ed.*, 2001, **40**, 3573.
- M. A. Carvajal, S. Álvarez and J. J. Novoa, *Chem.–Eur. J.*, 2004, **10**, 2117.
- A. Díez, E. Lalinde and M. T. Moreno, *Coord. Chem. Rev.*, 2011, **255**, 2426.
- E. J. Fernández, A. Laguna and J. M. López-de-Luzuriaga, *Dalton Trans.*, 2007, 1969.
- E. J. Fernández, A. Laguna and J. M. López-de-Luzuriaga, *Coord. Chem. Rev.*, 2005, **249**, 1423.
- Modern Supramolecular Gold Chemistry*, ed. A. Laguna, Wiley-VCH, 2008.
- E. J. Fernández, J. M. López-de-Luzuriaga, M. Monge, M. A. Rodríguez, O. Crespo, M. C. Gimeno, A. Laguna and P. G. Jones, *Chem.–Eur. J.*, 2000, **6**, 636.
- V. W. W. Yam and E. C. C. Cheng, *Chem. Soc. Rev.*, 2008, **37**, 1806.
- H. Schmidbaur and A. Schier, *Chem. Soc. Rev.*, 2008, **37**, 1931.
- S. Sculfort and P. Braunstein, *Chem. Soc. Rev.*, 2011, **40**, 2741.
- J. Forniés and A. Martín, in *Platinates (II) Complexes as Building Blocks for Complexes with Pt–M (Donor–Acceptor) Bonds*, ed. P. Braunstein, L. A. Oro and P. R. Raithby, Weinheim, 1999.
- J. Forniés, C. Fortuño, S. Ibáñez and A. Martín, *Inorg. Chem.*, 2008, **47**, 5978.
- J. Forniés, S. Fuertes, A. Martín, V. Sicilia, B. Gil and E. Lalinde, *Dalton Trans.*, 2009, 2224.
- J. Forniés, S. Ibáñez, A. Martín, B. Gil, E. Lalinde and M. T. Moreno, *Organometallics*, 2004, **23**, 3963.
- J. Forniés, S. Ibáñez, A. Martín, M. Sanz, J. R. Berenguer, E. Lalinde and J. Torroba, *Organometallics*, 2006, **25**, 4331.
- J. R. Berenguer, A. Díez, J. Fernández, J. Forniés, A. García, B. Gil, E. Lalinde and M. T. Moreno, *Inorg. Chem.*, 2008, **47**, 7703.
- J. M. Casas, J. Forniés, S. Fuertes, A. Martín and V. Sicilia, *Organometallics*, 2007, **26**, 1674.
- W. Chen, F. Liu, T. Nishioka and K. Matsumoto, *Eur. J. Inorg. Chem.*, 2003, 4234.
- A. Díez, J. Forniés, J. Gómez, E. Lalinde, A. Martín, M. T. Moreno and S. Sánchez, *Dalton Trans.*, 2007, 3653.
- T. Yamaguchi, F. Yamazaki and T. Ito, *J. Am. Chem. Soc.*, 1999, **121**, 7405.
- T. Yamaguchi, F. Yamazaki and T. Ito, *J. Am. Chem. Soc.*, 2001, **123**, 743.
- M.-E. Moret and P. Chen, *J. Am. Chem. Soc.*, 2009, **131**, 5675.
- G. Kampf, P. J. S. Miguel, M. Willermann, A. Schneider and B. Lippert, *Chem.–Eur. J.*, 2008, **14**, 6882.
- D. E. Janzen, L. F. Mehne, D. G. VanDerveer and G. J. Grant, *Inorg. Chem.*, 2005, **44**, 8182.
- S. A. Baudron and M. W. Hosseini, *Chem. Commun.*, 2008, 4558.
- G.-Q. Yin, Q.-H. Wei, L.-Y. Zhang and Z.-N. Chen, *Organometallics*, 2006, **25**, 580.
- M.-E. Moret and P. Chen, *Organometallics*, 2008, **27**, 4903.
- L. R. Falvello, J. Forniés, R. Garde, A. García, E. Lalinde, M. T. Moreno, A. Steiner, M. Tomás and I. Usón, *Inorg. Chem.*, 2006, **45**, 2543.
- O. Crespo, A. Laguna, E. J. Fernández, J. M. López-de-Luzuriaga, P. G. Jones, M. Teichert, M. Monge, P. Pyykkö, N. Runeberg, M. Schütz and H. J. Werner, *Inorg. Chem.*, 2000, **39**, 4786.
- The nature of these intermetallic Pt–Ag interactions has recently been studied on the basis of density functional theory (DFT) calculations on some related complexes (see ref. 24).
- L. R. Falvello, J. Forniés, A. Martín, V. Sicilia and P. Villarroya, *Organometallics*, 2002, **21**, 4604.
- E. Alonso, J. Forniés, C. Fortuño, A. Martín and A. G. Orpen, *Organometallics*, 2003, **22**, 5011.
- F. D. Rochon and R. Melanson, *Acta Crystallogr., Sect. C: Cryst. Struct. Commun.*, 1988, **44**, 474.
- L. R. Falvello, J. Forniés, C. Fortuño, F. Durán and A. Martín, *Organometallics*, 2002, **21**, 2226.
- I. Ara, L. R. Falvello, J. Forniés, J. Gómez, E. Lalinde, R. I. Merino and I. Usón, *J. Organomet. Chem.*, 2002, **663**, 284.
- L. R. Falvello, J. Forniés, E. Lalinde, B. Menjón, M. A. García Monforte, M. T. Moreno and M. Tomás, *Chem. Commun.*, 2007, 3838.
- G. J. Arsenault, C. M. Anderson and R. J. Puddephatt, *Organometallics*, 1988, **7**, 2094.
- P. T. Chou and Y. Chi, *Chem.–Eur. J.*, 2007, **13**, 380.
- M. W. Cooke and G. S. Hanan, *Chem. Soc. Rev.*, 2007, **36**, 1466.
- R. C. Evans, P. Douglas and C. J. Wiscom, *Coord. Chem. Rev.*, 2006, **250**, 2093.
- E. Holder, B. M. W. Langeveld and U. S. Schubert, *Adv. Mater.*, 2005, **17**, 1109.
- M. D. McClenaghan, N. D. Leydet, Y. Maubert, M. T. Indelli and S. Campagna, *Coord. Chem. Rev.*, 2005, **249**, 1336.
- S. S. Sun and A. J. Lees, *Coord. Chem. Rev.*, 2002, **230**, 171.
- W. Y. Wong, *Comments Inorg. Chem.*, 2005, **26**, 39.
- M. H. V. Huynh, D. M. Dattelbaum and T. J. Meyer, *Coord. Chem. Rev.*, 2005, **249**, 457.
- A. Vogler and H. Kunkely, *Top. Curr. Chem.*, 2001, **213**, 143.
- P. Thanasekaran, R. T. Liao, Y. H. Liu, T. Rajendran, S. Rajagopal and K. L. Lu, *Coord. Chem. Rev.*, 2005, **249**, 1085.
- Coord. Chem. Rev.*, 2000, **208** (special issue), 1.
- B. Ma, P. I. Djurovich and M. E. Thompson, *Coord. Chem. Rev.*, 2005, **249**, 1501.
- S. Pérez, C. López, A. Caubet, R. Bosque, X. Solans, M. F. Bardia, A. Roig and E. Molins, *Organometallics*, 2004, **23**, 224.
- J. R. Berenguer, E. Lalinde and M. T. Moreno, *Coord. Chem. Rev.*, 2010, **254**, 832.
- Z.-N. Chen, N. Zhao, Y. Fan and J. Ni, *Coord. Chem. Rev.*, 2009, **253**, 1.
- Z. N. Chen, Y. Fan and J. Ni, *Dalton Trans.*, 2008, 573.
- V. W. Yam and E. C. C. Cheng, *Chem. Soc. Rev.*, 2008, **37**, 1806.
- B. Ma, J. Li, P. I. Djurovich, M. Yousuffuddin, R. Bau and M. E. Thompson, *J. Am. Chem. Soc.*, 2005, **127**, 28.
- C.-K. Koo, Y.-M. Ho, C.-F. Chow, M. H.-W. Lam, T.-C. Lau and W.-Y. Wong, *Inorg. Chem.*, 2007, **46**, 3603.
- K. Saito, Y. Nakao and S. Sakaki, *Inorg. Chem.*, 2008, **47**, 4329.
- R. Usón, J. Forniés, M. Tomás, I. Ara, J. M. Casas and A. Martín, *J. Chem. Soc., Dalton Trans.*, 1991, 2253.
- L. R. Falvello, J. Forniés, A. Martín, V. Sicilia and P. Villarroya, *Organometallics*, 2002, **21**, 4604.
- I. Ara, J. Forniés, V. Sicilia and P. Villarroya, *Dalton Trans.*, 2003, 4238.
- J. R. Berenguer, B. Gil, J. Fernández, J. Forniés and E. Lalinde, *Inorg. Chem.*, 2009, **48**, 5250.
- A. Díez, A. García, E. Lalinde and M. T. Moreno, *Eur. J. Inorg. Chem.*, 2009, 3060.
- J. Forniés, S. Fuertes, J. A. López, A. Martín and V. Sicilia, *Inorg. Chem.*, 2008, **47**, 7166.
- A. R. Dick, J. W. Kampf and M. S. Sanford, *Organometallics*, 2005, **24**, 482.
- J. De Priest, G. Y. Zheng, C. Woods, D. P. Rillema, N. A. Mikirova and M. E. Zandler, *Inorg. Chim. Acta*, 1997, **264**, 287.
- N. Godbert, T. Pugliese, I. Aiello, A. Bellusci, A. Crispini and M. Ghedini, *Eur. J. Inorg. Chem.*, 2007, 5105.
- A. Díez, J. Forniés, A. García, E. Lalinde and M. T. Moreno, *Inorg. Chem.*, 2005, **44**, 2443.
- P. Jolliet, M. Gianini, A. von Zelewsky, G. Bernardinelli and H. Stoeckli-Evans, *Inorg. Chem.*, 1996, **35**, 4883.
- D. E. Janzen, D. G. VanDerveer, L. F. Mehne, D. A. da Siva Filho, J. L. Bredas and G. J. Grant, *Dalton Trans.*, 2008, 1872.
- M. Munakata, L. P. Wu and G. L. Ning, *Coord. Chem. Rev.*, 2000, **198**, 171.
- S. Q. Liu, T. Kuroda-Sowa, H. Konaka, Y. Suenaga, M. Maekawa, T. Mizutani, G. L. Ning and M. Munakata, *Inorg. Chem.*, 2005, **44**, 1031.
- Y.-B. Dong, Y. Geng, J.-P. Ma and R.-Q. Huang, *Inorg. Chem.*, 2005, **44**, 1693.
- Y.-B. Dong, G.-X. Jin, X. Zhao, B. Tang, R.-Q. Huang, M. D. Smith, K. E. Stitzer and H.-C.-. zur Loye, *Organometallics*, 2004, **23**, 1604.
- A. P. Côté and G. K. H. Shimizu, *Inorg. Chem.*, 2004, **43**, 6663.

- 77 T. Brasey, A. Buryak, R. Scopelliti and K. Severin, *Eur. J. Inorg. Chem.*, 2004, 964.
- 78 D. Braga and F. Grepioni, *Chem. Soc. Rev.*, 2000, **29**, 229.
- 79 R. Usón, J. Forniés, L. R. Falvello, M. Tomás, J. M. Casas and A. Martín, *Inorg. Chem.*, 1993, **32**, 5212.
- 80 J. P. H. Charmant, J. Forniés, J. Gómez, E. Lalinde, R. I. Merino, M. T. Moreno and A. G. Orpen, *Organometallics*, 1999, **18**, 3353.
- 81 V. W. Yam, K. L. Yu and K. K. Cheung, *J. Chem. Soc., Dalton Trans.*, 1999, 2913.
- 82 B. Gil, J. Forniés, J. Gómez, E. Lalinde, A. Martín and M. T. Moreno, *Inorg. Chem.*, 2006, **45**, 7788.
- 83 R. Usón, A. Laguna, M. Laguna, B. R. Manzano, P. G. Jones and G. M. Sheldrick, *J. Chem. Soc., Dalton Trans.*, 1984, 285.
- 84 B. Norén and A. Oskarsson, *Acta Chem. Scand.*, 1984, **38**, 479.
- 85 E. J. Fernández, A. Laguna, J. M. López-de-Luzuriaga, M. Montiel, M. E. Olmos, J. Pérez and R. C. Puelles, *Organometallics*, 2006, **25**, 4307.
- 86 M. Bardají, O. Crespo, A. Laguna and A. K. Fischer, *Inorg. Chim. Acta*, 2000, **304**, 7.
- 87 J. M. Casas, J. Forniés, A. Martín, B. Menjón and M. Tomás, *Polyhedron*, 1996, **15**, 3599.
- 88 E. J. Maslowsky, *Vibrational Spectra of Organometallic Compounds*, Wiley, 1977.
- 89 *SAINT Program for X-ray data integration version 5.0*, Bruker Analytical X-ray Systems, Madison, WI, 2000.
- 90 G. M. Sheldrick, *SADABS, Program for area detector adsorption correction*, Institute for Inorganic Chemistry, University of Göttingen, Germany, 1996.
- 91 *CrysAlis RED Program for X-ray CCD camera data reduction*, Oxford Diffraction Ltd, Oxford, UK, 2008.
- 92 G. M. Sheldrick, *SHELXL-97, Program for refinement of crystal structures*, University of Göttingen, Germany, 1997.
- 93 J. P. Perdew, K. Burke and M. Ernzerhof, *Phys. Rev. Lett.*, 1996, **77**, 3865.
- 94 M. J. Frisch *et al.*, *Gaussian 03, revision E.01*, Pittsburgh, PA, 2003.